Hybrid nano- and microgels doped with photoacoustic contrast agents for cancer theranostics

Yu Xiao, Jérôme Gateau, Amanda K A Silva, Xiangyang Shi, Florence Gazeau, Claire Mangeney, Yun Luo

Received: 21 February 2021 | Revised: 12 May 2021 | Accepted: 31 May 2021

DOI: 10.1002/VIW.20200176

REVIEW

Hybrid nano- and microgels doped with photoacoustic contrast agents for cancer theranostics

Yu Xiao[1] | **Jérôme Gateau**[2] | **Amanda K A Silva**[3] | **Xiangyang Shi**[4] | **Florence Gazeau**[3] | **Claire Mangeney**[1] | **Yun Luo**[1]

[1] LCBPT, CNRS UMR 8601, Université de Paris, Paris, France

[2] CNRS, INSERM, Laboratoire d'Imagerie Biomédicale, LIB, Sorbonne Université, Paris, France

[3] MSC, CNRS UMR 7057, Université de Paris, Paris, France

[4] College of Chemistry, Chemical Engineering and Biotechnology, Donghua University, Shanghai, P. R. China

Correspondence
Florence Gazeau, MSC, CNRS UMR 7057, Université de Paris, 45 rue des Saints-Pères, Paris, 75006, France.
Email: florence.gazeau@u-paris.fr
Claire Mangeney, LCBPT, CNRS UMR 8601, Université de Paris, 45 rue des Saints-Pères, Paris, 75006, France.
Email: Claire.mangeney@u-paris.fr
Yun Luo, LCBPT, CNRS UMR 8601, Université de Paris, 45 rue des Saints-Pères, Paris, 75006, France.
Email: yun.luo@u-paris.fr

Funding information
Agence Nationale de la Recherche, Grant/Award Number: ANR-18-IDEX-0001; Region Ile de France

Abstract

Photoacoustic imaging (PAI) is an emerging noninvasive and inexpensive bioimaging modality, which has stimulated a wide interest in recent years for cancer theranostics. Hybrid nano- and microgels have been designed as protective carriers to incorporate PAI contrast agents due to their biocompatibility and biodegradability, high loading capacity, versatile surface chemistry, and stimuli-responsive properties. These key features offer unprecedented opportunities for the design of innovative multifunctional cancer theranostic agents. This review focuses on the recent development of photoacoustic active nano- and microgels for biomedical applications in cancer theranostics and cancer hallmark imaging. The various chemical natures of gels and PAI contrast agents and the elaboration methods of hybrid matrices are summarized and discussed. Their applications in multimodal cancer theranostics and cancer hallmark imaging are presented, highlighting their merits and potential in treatment and diagnosis.

KEYWORDS
cancer theranostics, contrast agents, hybrid microgels, nanoparticles, photoacoustic imaging

1 | INTRODUCTION

Imaging in medical oncology has recently experienced major breakthrough with the arrival of new molecular imaging techniques devoted to the early diagnosis of cancer and to treatment monitoring. In particular, photoacoustic imaging (PAI) has stimulated a wide interest in the medical imaging community due to its considerable capabilities for cancer physiological and molecular imaging. PAI is a hybrid imaging technique, based on the photoacoustic effect, which combines optical excitation and ultrasound detection. The PA mechanism, which

was firstly observed by A. G. Bell in 1880,[1] is based on the local absorption of an incident nonionizing light pulse, followed by the rapid and transient heating of the surrounding biological tissues and its thermoelastic expansion. This expansion generates ultrasound waves that originate from the optical absorbers inside the tissue and propagate outwards to the tissue surface where they can be detected and then analyzed using image reconstruction techniques to yield optical absorption maps. As a multiwave imaging technique, PAI offers two key advantages over single-wave methods.[2–4] First, compared to purely optical imaging techniques, it offers large imaging depth (up to 4-5 cm in vivo[5] and 11-12 cm in vitro) and high spatial resolution (depth-resolution ratio approximately 200,[6] approximately 100 μm at cm depth). This is achieved thanks to the combination of the relatively high tissue penetration of near infrared (NIR)[7] excitation (from 650 to 1700 nm) and the low scattering of the acoustic waves (in the MHz range) in tissue. Second, compared to ultrasound imaging, PAI offers a high and rich optical contrast, which enables to separate absorbing structures from the background and to distinguish absorbers based on their absorption spectra.[8] Endogenous absorbing molecules, such as oxy- and deoxy-hemoglobin and melanin, have been efficiently used for the visualization of vessel structures, the quantification of blood oxygenation and the detection of melanoma.[9,10] However, only few types of endogenous biomolecules can be exploited for intrinsic PAI, limiting its range of applications. To overcome these barriers and boost PAI specificity, many efforts have been devoted to the development of exogenous contrast agents. These materials, usually based on NIR absorbing dyes or nanomaterials, are able to extend the application of PAI in cancer theranostics. For example, metallic, carbon, or semiconducting polymer nanoparticles (NPs), and molecular dyes (eg, indocyanine green, fluorescent proteins) have been reported for in vivo PA tumor imaging.[11] Nevertheless, it remains a great challenge to efficiently deliver PA contrast agent to their targets, owing to their unstable chemical properties and short circulation lifetime.[12] To overcome these issues, biocompatible, hydrophilic, and protective delivery vehicles with prolonged blood circulation lifetimes are highly desirable. Cross-linked hybrid nano- and microgels can fulfill the demands thanks to their: (i) high loading capacity (eg, imaging agent, drugs, etc.); (ii) versatility for surface modification (eg, by targeting molecules) and rapid response to external stimuli (eg, pH, temperature, etc.). These merits favor the targeting and controlled release of guest agents,[13] efficiently improving cancer diagnosis and therapy (Figure 1). Besides, hybrid nano- and microgels exhibit prolonged blood circulation time, which is highly suitable for theranostic agent delivery.

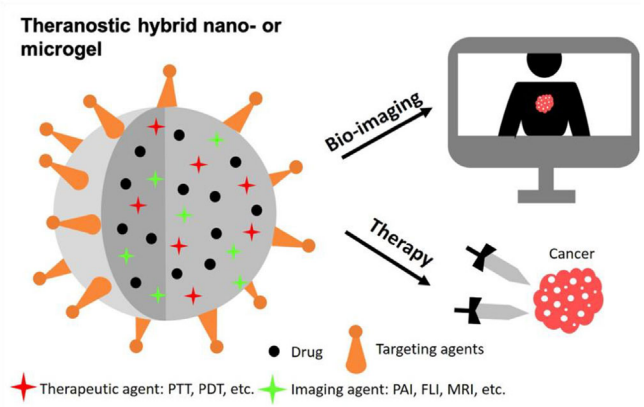

FIGURE 1 Illustration of theranostic agent based on hybrid microgel encapsulating imaging and therapeutic agents for cancer diagnosis and therapy. FLI, fluorescence imaging; MRI, magnetic resonance imaging; PAI, photoacoustic imaging; PDT, photodynamic therapy; PTT, photothermal therapy.

For example, poly(*N*-isopropylacrylamide-*co*-acrylic acid) nanogels loaded with Fe_3O_4 NPs and conjugated with Cy5.5-labeled lactoferrin, designed for targeted glioma imaging, exhibited longer blood retention time (half-life period = 5.3 h) with respect to free contrast agent (half-life period = 2.2 h) in rat models.[14] In another example, zwitterionic poly(phosphorylcholine) based nanogels could largely prolong the blood circulation time of anticancer drug (Cy5).[15] Forty eight hours after the first intravenous injection in BALB/c mice, more than 20% of Cy5 injection dose could be detected in the blood for the nanogel-Cy5 composite, whereas only less than 5% was found for free Cy5. Similar results were observed 48 h after the second intravenous injection. Therefore, nano- or microgels (10-200 nm) carriers have attracted lots of interests, due to their longer circulating time in blood, allowing more theranostic agents to be passively delivered and accumulate in tumor tissue after intravenous injection.[16]

In this review, we introduce the basic concepts for the design of hybrid microgels in the domain of PAI. The methods to synthesize hybrid assemblies are described and their applications in cancer-related PAI and biomedicine are summarized focusing on two main orientations: (i) multimodal cancer theranostics including PAI or/and synergistic therapy; and (ii) cancer hallmark detection and microenvironment investigation using PAI.

2 | CHEMICAL NATURE OF HYBRID MICROGELS FOR PA IMAGING

2.1 | Polymer nano- and microgels

Various polymer nano- or microgels have been used to load contrast agents for PAI in oncology. They can

be classified into two categories: (i) biopolymers or (ii) synthetic polymer particles, as listed Tables 1 and 2. For example, engineered polypeptide ($PC_{10}A$) expressed on *Escherichia Coli* has been purified and loaded with PAI contrast agents.[17–19] Hyaluronic acid derivatives,[20] chitosan,[21] gelatin,[22] and polyglutamic acid,[12,23] have been used for the design of multimodal cancer theranostic platforms. Biopolymers exhibit excellent biodegradability, biocompatibility, and low immunogenicity. However, some of them (eg, engineered polypeptide) require complex preparation and purification processes, with potential risk of batch-to-batch variation. Moreover, some natural polymers possess a few types of terminated functional groups, such as dextran, which has only -OH termini. This might limit the diversity of their possible postfunctionalization or conjugation reactions. Alternatively, synthetic polymers based on polyethylenimine,[24] polyethylene glycol,[25–27] polypyrrole,[28] poly(acrylic acid),[29–31] and polyglycerol[32] have been reported as scaffolds for PAI contrast agent delivery. The advantages of synthetic polymers are their controllable physicochemical (eg, size, shape, etc.) and surface properties (eg, surface charge, functional groups for conjugation, etc.), favoring the elaboration of multifunctional and multimodal system for bioimaging and therapy. Nevertheless, synthetic polymers might be nonbiodegradable, as for example, PHPMA (poly (*N*-(2-(hydroxypropyl) methacrylamide), even though it has been applied in prototype anticancer treatment.[33,34] Therefore, one should carefully design and select proper synthetic polymers for drug delivery.

2.2 | Synthesis of hybrid nano- and microgels for PAI

The elaboration of hybrid nano- and microgels for PAI can be achieved by three main approaches (cf. Figure 2): (i) the in situ synthesis of contrast agents inside the hydrogel microparticle matrix; (ii) the formation of gel particles from PA active monomers/initiators/crosslinkers; (iii) the ex situ self-assembly of microgels and contrast agents. In the first method, the precursors are mixed with nano- or microgels, followed by contrast agent's generation process. For example, CuS NPs could be in situ synthesized in theranostic microgels by mixing Cu^{2+} precursors with gels, followed by reaction with Na_2S.[24] Another example is the in situ polymerization of polyaniline (PANI) in microgels from preloaded aniline monomers.[12] Besides, nanogels made of copper methacrylate crosslinkers can act as precursors to generate in situ CuS NPs.[27] In the second approach, PA active monomers, such as pyrrole,[28] were used for the formation of microgels. Monomers could be also prefunctionalized by PA dye molecules, such as

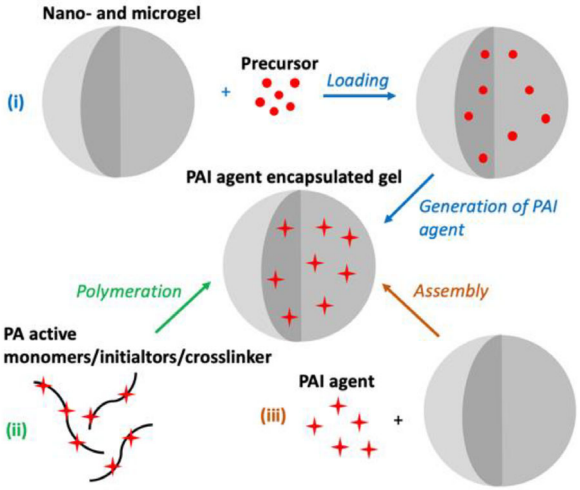

FIGURE 2 Illustration of the various elaboration strategies for designing hybrid nano- and microgels loaded with PAI contrast agents

oxyphor G2,[35] for the in situ generation of gel matrix. In the third method, hybrid nano- and microgels can be prepared by the ex situ self-assembly of gel matrix and contrast agents, relying on attractive interactions such as electrostatic forces, π–π stacking, H-bonding, or covalent grafting. For example, Ag_2S NPs could be encapsulated into polypeptides.[18,19] Methylene blue was loaded into cisplatin-modified gelatin nanogels.[22] Indocyanine was loaded to polydopamine-coated PEGylated polypyrrole nanogels.[30] The first and second approaches described above are rapid and offer a simple way to generate hybrid gels. However, the morphology and properties of contrast agents (for the first method) and gel particles (for the second method) are hard to control. Regarding the ex situ generation approach (third method), it requires distinct stages to prepare separately the contrast agents and gels, and assemble them into hybrid particles, which can lead to longer procedures. Yet the size, shape and surface properties of each separate component can be defined and controlled more accurately.

2.3 | PAI contrast agents

Different types of PAI contrast agents have been loaded within polymer micro- or NPs. They can be divided into three main categories (Figure 3): (i) molecular dyes; (ii) inorganic nanomaterials; (iii) semiconducting polymers.

Molecular dyes have been widely used in PAI due to their low toxicity and commercial availability. Commonly used dyes include cyanines, Evens blue and methylene blue, .[36–39] Nevertheless, major limitations hinder their application in clinics, such as their poor aqueous solubility and

TABLE 1 Hybrid microgels for cancer photoacoustic imaging and theranostics

Microgel scaffold	Imaging agent	Phototherapy agent	Targeting agent	Chemotherapeutic drug	Particle size	Administration mode	Refs.
Biopolymer gel matrix							
Polypeptides ($PC_{10}A$)	Ag_2S quantum dots for PAI and FLI	Ag_2S quantum dots for PTT	Arginyl-glycyl-aspartic acid (RGD)	–	$D_h \approx 160$ nm	Intratumoral injection	[18]
Dextran-polypyrrole	Polypyrrole (PPY) for PAI	PPY for PTT	–	–	$D_h \approx 93$ nm	Intratumoral injection	[28]
γ-Polyglutamic acid (γ-PGA)	Polyaniline (PANI) for PAI	PANI for PTT	–	–	$D = 71.9 \pm 15.8$ nm	Intratumoral injection	[12]
γ-PGA	PPY for PAI	PPY for PTT	–	–	$D = 38.9 \pm 8.6$	Intratumoral injection	[23]
Gelatin	Methylene blue for PAI and FLI	Methylene blue for PTT and PDT	–	Cisplatin	$D_h = 146.3 \pm 5.0$ nm	Intravenous injection	[22]
Chitosan	Carbon quantum dots for PAI and FLI	Carbon quantum dots for PTT	–	Doxorubicin	$D_h = 78$ nmD $\approx$ 65 nm	Intravenous injection	[21]
Janus-type hyaluronic acid derivatives	Indocyanine green for PAI and FLI	–	–	–	$D_h = 157$-209 nm	Intravenous injection	[20]
Polypeptides ($PC_{10}A$)	Ag_2S quantum dots for PAI for FLI	Ag_2S quantum dots for PTT	–	Paclitaxel	$D = 85 \pm 15$ nm	Intratumoral injection	[19]
Chemical polymer gel matrix							
Polyethylenimine	CuS for PAI and Gd^{3+} for MRI	CuS for PTT	Folic acid	–	$D_h = 150$ nm	Intravenous injection	[24]
PEGylated polypyrrole	Indocyanine green for PAI	Indocyanine green for PTT	–	–	$D = 65$ nm$D_h = 331.3 \pm 3.7$ nm	Intravenous injection	[25]
Terrylenediimide-poly(acrylic acid)	Terrylenediimide for PAI	Terrylenediimide for PTT	–	–	$D = 10 \pm 1.2$ nm$D_h = 12.6 \pm 2.3$ nm	Intravenous injection	[29]
Core-shell silica-polyethylene glycol	Cyanine 5.5 and 7 for PAI, FLI	Cyanine 5.5 and 7 for PTT	–	–	$D \approx 10$ nm$D_h \approx 30$ nm	–	[26]
Polystyrene-b-poly (*N*-isopropylacrylamide-*co*-acrylic acid)	Diketopyrrolo-pyrrole for PAI	Diketopyrrolo-pyrrole for PTT	–	Doxorubicin	$D_h = 75$ nm	Intravenous injection	[30]
Copolymers of polymethacrylic acid and poly(ethylene glycol) methacrylate	CuS for PAI	CuS for PTT	–	Doxorubicin	$D_h \approx 95$ nm	Intravenous injection	[27]
Polyglycerol	PPY for PAI	PPY for PTT	–	Methotrexate	$D_h = 176$-244 nm	Intravenous injection	[32]

D, mean particle diameter determined from electronic microscopy; D_h, mean hydrodynamic diameter; FLI, fluorescence imaging; PAI, photoacoustic imaging; PDT, photodynamic therapy; PTT, photothermal therapy.

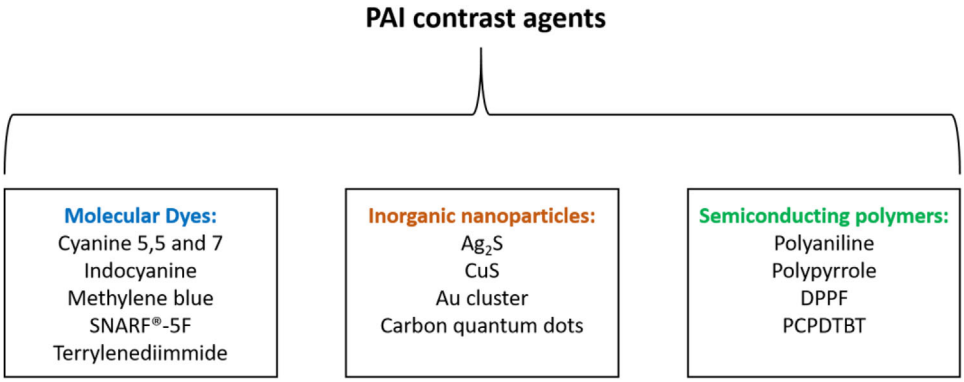

FIGURE 3 PAI contrast agents for multimodal cancer theragnostic and cancer hallmark imaging. SNARF®, seminaphtharhodafluor; DPPF, poly[3-(5-(9-hexyl-9-octyl-9H-fluoren-2-yl) thiophene-2-yl)-2,5-bis(2-hexyldecyl)-6-(thiophene-2-yl)pyrrolo[3,4-c]pyrrole-1,4(2H,5H)-dione]; PCPDTBT, poly[2,6-(4,4-bis(2-ethylhexyl)-4H-cyclopenta[2,1-b;3,4-b′]dithiophene)-alt-4,7(2,1,3benzothiadiazole)]

short circulation time in vivo. To overcome these barriers, small molecular dyes were loaded within microgels, acting as carriers to increase the PAI contrast agent availability and improve targeting efficacy. For example, Zhai and colleagues designed multifunctional nanovesicles (MPV) based on cell membrane shells and gelatin nanogel cores to coload methylene blue and cisplatin (Pt).[22] Core-shell silica-polyethylene glycol NPs were doped with Cyanines 5.5 and 7 to provide fluorescent, photoacoustic, and photothermal capabilities in vitro on MDA-MB-231 cancer cells.[26] Indocyanine functionalized polypyrrole NPs have been designed for PAI and PTT on HeLa tumor bearing nude mice.[][25]

Inorganic nanomaterials based on plasmonic NPs have also stimulated a wide interest for PAI due to their remarkable optical properties arising from localized surface plasmon (LSP). In particular, their optical absorption cross-sections are several order of magnitude larger than those of small molecular dyes.[40] Therefore, these NPs can release heat energy upon LSP excitation, resulting in light-to-heat conversion, which was exploited for PAI and photothermal therapy applications. However, it is still a great challenge to apply plasmonic colloids (eg, Au NPs and Ag NPs) in clinics because the LSP resonance of simple spherical gold or silver NPs can be only excited in the visible range (400-600 nm), where the strong absorbance of the hemoglobin limits the penetration depth to the millimeter range. Fortunately, LSP properties can be adjusted by modifying NP morphology, structure, and coupling in order to shift the excitation wavelength to the NIR region. For example, Chen et al. designed nanocomposites based on thermoresponsive poly(*N*-isopropylacrylamide) (PNIPAM) nanogels embedding gold nanorods (AuNR) and CuS NPs as nanoheaters.[41] In another example, densly packed sub-5 nm Au NPs were encapsulated into reactive oxygen species (ROS) sensitive polyphosphazene nanogels for ROS imaging in cancer microenvironment.[42] NIR-absorbing Ag_2S and CuS loaded gel matrix have been applied for cancer PAI and PTT.[18],[27] Besides, carbon-based nanomaterials, such as carbon quantum dots, carbon nanotubes and graphene, have been also reported for PAI.[21],[43-45] Although they exhibit lower molar extinction coefficients compared to plasmonic NPs, carbon-based nanomaterials offer valuable advantages for PAI including ease of fabrication and surface functionalization.

Semiconducting polymers have emerged prominently in PAI due to their high absorption coefficient, strong photostability, adjustable optical properties, and controllable size.[46,47] This kind of contrast agent is mainly made of semiconducting polymers composed of biologically inert components, thus, exhibiting good biocompatibility.[46] For example, PANI functionalized nanogels have been reported for PAI-guided PTT of tumors.[12] Terrylenediimide-based polymeric NPs with high photothermal conversion effect have been studied in PAI and PTT.[29] Polypyrrole-loaded nanogels could enhanced PA intensity, favoring tumor photothermal ablation.[23]

3 | APPLICATIONS IN THERANOSTICS AND CANCER HALLMARK IMAGING

3.1 | Multimodal cancer theranostics

Most PAI contrast agents exhibit photothermal effect, converting the absorbed light into heat. As a result, the surrounding temperature can be increased and cause cell death or/and tissue ablation. The treatment based on photothermal effect is called photothermal therapy or hyperthermia in clinical setting.[48] It is a minimally invasive

TABLE 2 Hybrid microgels for cancer hallmark photoacoustic imaging

Microgel scaffold	PAI agent	Method	Hallmark	Particle size	Administration	Refs.
Polyacrylamide (PAA)	SNARF®-5F	Ratiometric PA signal of pH-sensitive SNARF-5F at 600 and 565 nm	pH value changes	$D_h \approx 60$ nm	Intravenous injection	[31]
PAA	oxyphor G2 dye	PA life time of G2 dye related to surrounding O_2 concentration	Low oxygen concentration (hypoxia)	$D_h \approx 60$ nm	Intravenous injection	[35]
DPPF and PCPDTBT	DPPF, PCPDTB	PA sensing: signal increasing when probe binding to protein sulfonic acid.	Oxidative stress	$D_h \approx 18$ nm	Intravenous injection	[60]
PCCP and PPB	AuNPs	PA signal sensing: signal decreasing in case of reactive oxygen species	Reactive oxygen species	$D = 142.1 \pm 38.2$ nm	–	[42]

D, mean particle diameter determined from electronic microscopy; D_h, mean hydrodynamic diameter; DPPF, Poly[3-(5-(9-hexyl-9-octyl-9H-fluoren-2-yl)thiophene-2-yl)-2,5-bis(2-hexyldecyl)-6-(thiophene-2-yl)pyrrolo[3,4-c]pyrrole-1,4(2H,5H)- dione]; PAA, polyacrylamide; PCPFTBT, poly[2,6-(4,4-bis(2-ethylhexyl)-4H-cyclopenta[2,1-b;3,4-b']dithiophene)-alt-4,7(2,1,3-benzothiadiazole)]; PCCP, poly[di(carboxylatophenoxy) phosphazene]; PPB, arylboronate polyphosphazene derivative; SNARF, seminaphtharhodafluor.

way to treat cancer. The simultaneous use of PAI/PTT has attracted great interest for theranostics. Both inorganic and organic PAI contrast agents can be applied for PTT, as overviewed in recent reviews.[49,50] For example, organic dyes (eg, methylene blue, indocyanine green)[22],[51] or polymers (eg, PANI and polypyrrole)[52,53] have been reported as simultaneous PAI/PTT agents. Alternatively, inorganic materials, such as carbon nanomaterials (eg, carbon dots, graphene),[43],[54] plasmonic (eg, Au),[56,57] and semiconducting NPs (eg, Ag_2S, CuS),[55]–[58,59] have been used.

Interestingly, the encapsulation of PAI/PTT theranostic agents within smart microgels offers unprecedented opportunities to control their delivery, release, or/and biodistribution, favoring cancer diagnosis and therapy.[13] Therefore, such a multimodal system is receiving more and more attention. As summarized in Table 1, these multimodal theranostic systems can be obtained either by: (i) loading simultaneously PAI and PTT agents in microgels with[18], [24] or without[12],[23],[26],[28-30] tumor targeting agent on the surface or (ii) by coencapsulating PAI/PTT agents with chemotherapeutic molecules, improving cancer treatment efficiency.[19],[21],[22],[27],[30],[32] PAI agents based on organic dyes, such as cyanine[20,26] and methylene blue derivatives[22] or NPs, such as carbon quantum dots,[21] and Ag_2S,[18] have intense fluorescence emission, which could be applied for dual-mode PAI-fluorescence imaging. In addition, microgels are able to carry a secondary imaging agent (such as Gd^{3+} complex for MRI) together with PAI agent, forming multimodal imaging system and boosting diagnostic accuracy.[24] Besides, it is possible to establish dual phototherapy, namely, PTT and photodynamic therapy (PDT), if the PAI agents release ROS under laser excitation. For example, a versatile theranostic system has been reported to encapsulate methylene blue and cisplatin in gelatin.[22] In this work, methylene blue is responsible for both imaging (eg, PAI and fluorescence imaging) and phototherapy (eg, PTT and PDT). Combined with anticancer drug (eg, cisplatin), localized hyperthermia, PDT, and chemotherapy, this multifunctional theranostic agent can efficiently kill 4T1 breast cancer cells leading to primary tumor regression and 97% inhibition of pulmonary metastasis.

3.2 | Applications in cancer hallmark imaging

The hallmarks of cancer, first described by Hanahan and Weinberg,[61] constitute common traits and key mechanisms underpinning all cancers including insensitivity to antigrowth signals, evasion of apoptosis, limitless replicative potential, sustained angiogenesis, tissue inva-

sion, and metastasis. Additional characteristic features of cancers are related to the tumor microenvironment,[62] such as reprogramming energy metabolism, evading immune response, extracellular matrix remodeling, aberrant vascularization, hypoxia, and genome instability and mutation.[62,63] Imaging techniques offer unique opportunities to investigate most of these tumor-related characteristics and provide a noninvasive anatomic, physiologic, and molecular assessment of tumor biology for clinical practice and disease treatment. Therefore, great efforts have been devoted to the detection and imaging of cancer hallmarks. In this section, we will focus on the use of PAI for assessing cancer hallmarks such as pH, oxygen changes, oxidative stress, and ROS production (as summarized in Table 2). The detection of these traits are usually based on MRI,[64,65] PET,[66,67] and fluorescent optical imaging.[68–70] However, MRI and PET are expensive techniques, and are not recommended for patients with pregnancy, breastfeeding, or with metal implants. In alternative, optical imaging and ultrasound techniques are noninvasive, low cost, and easy to use. Nevertheless, fluorescence imaging measurements are not suitable for deep tissue analysis due to the strong optical scattering in tissue, limiting spatial resolution for in vivo imaging. As ultrasound scattering is 100 to 1000 times weaker than optical scattering, PAI allows improving spatial resolution deeply in tissue.

pH value changes occur in tumor due to altered metabolic state, from aerobic glycolysis to anaerobic glycolysis.[71] This metabolic pathway produces excess lactic acid, leading to acidic microenvironment, which can be related to local recurrence, metastasis, and failure of chemotherapy.[72–74] Therefore, it is very important to establish applicable clinical tools to obtain quantitative pH information in tumor.

The use of PAI for pH sensing has been reported,[7],[75-77] using molecular pH-indicators, exhibiting pH-dependent absorption spectra in NIR. However, this approach does not allow accurate in vivo tumor pH imaging because the free molecular contrast agents may also interact with various biomolecules (eg, proteins, enzymes, etc.), that could modify their optical properties. Moreover, the strong presence of hemoglobin in biological tissues and its absorption spectra may prevent a simple amplitude-based discrimination of the contrast agent in the image, calling for the use of additional spectral discrimination. Wang and coworkers reported the design of polyacrylamide (PAA) NPs encapsulating molecular contrast agents (eg, SNARF®-5F) for PA pH imaging (Figure 4A).[31] The PAA served as a matrix to load SNARF-5F, improving biocompatibility[13] and preventing interaction between biomolecules and dyes.[31] The NPs were also functionalized by tumor targeting F_3 peptides to target cancer cells. As shown in Figure 4B, the absorption band of SNARF-PAA NPs shifted in the visible range from 565 nm at pH = 6 to 600 nm at pH 8 (pK_a = 7.2[78]), providing an easy means to use the ratio of the PA absorption intensities at the two absorption wavelengths for pH measurement at millimeter depths. Interestingly, a ratiometric method was proposed to discriminate the contributions of hemoglobin and the SNARF®-PAA NPs with as few as four excitation wavelengths. From Figure 4C, PA signal can be clearly distinguished at different pH in the presence of 1% whole blood, regardless the concentration of SNARF®-PAA loading, in the concentration range of 2-20 mg/mL. In vivo PA pH imaging performed 75 min after injection, showed that, the pH value was lower in tumor (Figure 4D) with respect to normal tissue (Figure 4E), evidencing a pH contrast between the center area (solid line) of the tumor and the peripheral part (dash line).

Low oxygen concentration (hypoxia) is also a characteristic of tumor microenvironment, associated with cancer pathologies.[79–81] PA oxygen imaging can firstly be based on endogenous hemoglobin, which absorption band changes upon binding/unbinding to oxygen.[82] However, hemoglobin gives only blood oxygen levels which provides an indirect information on the oxygen level in extravascular tumor tissues. Therefore, new PA contrast agents are desired to achieve direct tumor oxygen mapping. Recently, Kopleman and coworkers reported a PA life time (PALT) method for tumor oxygen imaging based on PAA nanogels doped with oxyphor G2 dye,[35] noted as G2-PAA NPs in Figure 5A. The hydrogels, functionalized by tumor-homing peptides, allowed the transport of the dye molecules to the target while protecting them from the interferences with biological species (such as proteins). The phosphorescent G2 molecules act as light absorbers whose absorbance decays over time with an exponential decay rate proportional to the oxygen concentration, after they have been excited with a pump laser pulse. The decay is evaluated with PAI by probe laser pulses at a different wavelength than the pump pulse. Varying delay times between pump and probe laser pulses (Figure 5B and C) allowed to assess the transient absorption and its decay rate and thereby the oxygen concentration. As shown in Figure 5D, the linear fit of the decay rate was similar for 2, 5, and 20 mg/mL of G2-PAA NPs with/without human serum albumin, indicating that the oxygen concentration measurements is independent of NPs concentration and surrounding biological species. In mouse model, the PA images showed that NPs accumulate in the tumor region after 60 min of injection (Figure 5E). The PALT oxygen imaging showed low oxygen concentration in tumor (dashed cycle, Figure 5F) compared to normal tissue, as shown in Figure 5G.

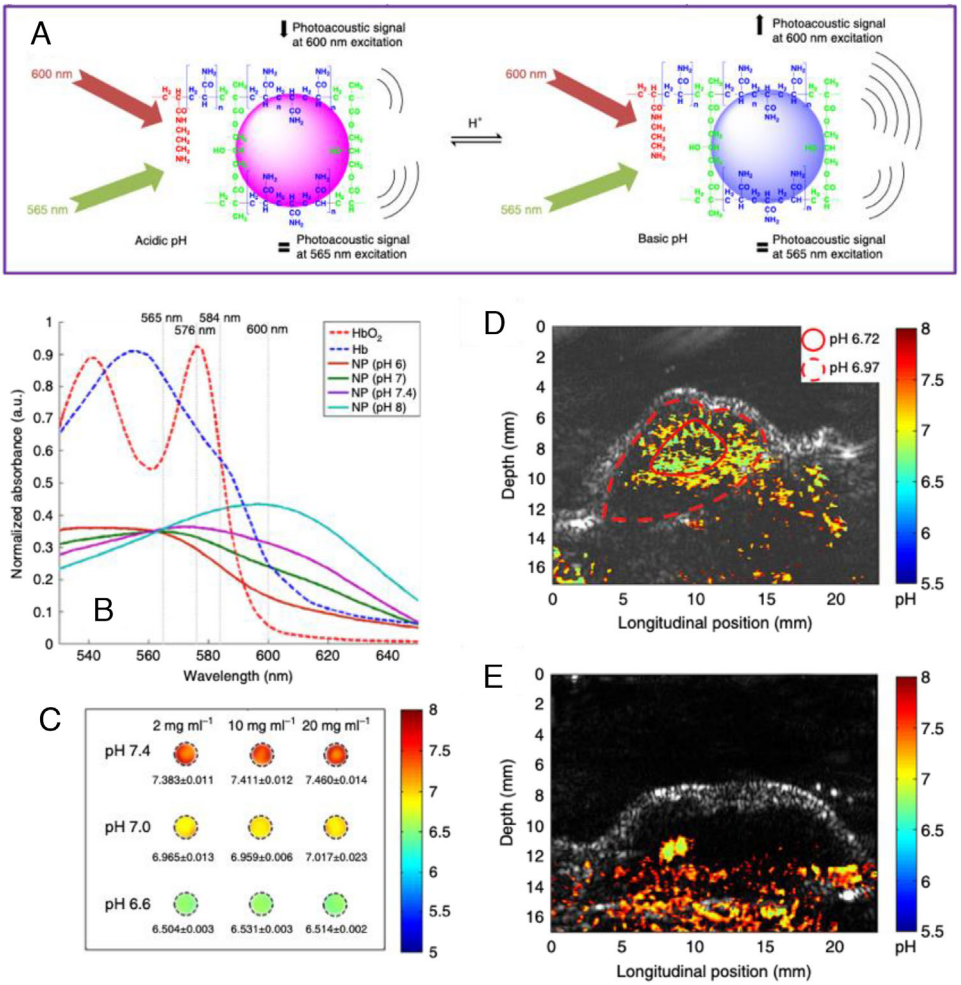

FIGURE 4 (A) Illustration of the pH-sensing mechanism of SNARF-PAA NPs, based on PA signals. The PA signal intensity at 600 nm is pH-dependent whereas that at 565 nm is constant. The ratio of signal at 600 nm over that at 565 nm, chosen as an internal reference changes with pH variations. (B) UV-vis spectra of SNARF-PAA NPs, HbO_2, and Hb. (C) Results of the four-wavelength ratiometric pH imaging at pH = 6.6, 7.0, and 7.4, using 2, 10, and 20 mg/mL of NPs in presence of 1% whole blood. In vivo pH imaging in mouse model 75 min after injection of SNARF-PAA (20 mg/mL) for (D) tumor and (E) normal tissue. Reprinted with permission from Ref. [31]. Copyright (2017) Spinger Nature

Oxidative stress, is another hallmark of cancer,[83,84] related to damaging effects caused by the production of ROS through disturbed redox state of cells. The formation of protein sulfonic acid (R-SOH), based on thiol oxidation in cell, is an indicator of damage caused by ROS. The detection of protein sulfonic acid is usually based on its interaction with a chemical probe, such as derivatives of dimedone (5,5-dimethyl-1,3-cyclohexanedione), which can be monitored by fluorescence spectroscopy, for in vitro detection.[69],[85] *Pu* et al. developed a PA method for the detection of R-SOH in vivo.[60] In this work, a core-shell nanocomposite (rSPN) was prepared using PA active polymers (SP2) cores coated by silica shells, functionalized by a chemical probe (Dyn-2, dimedone derivatives), which allow chemical binding to R-SOH, as shown in Figure 6A. The PA signal of rSPN2 (composite based on SP2 contrast agent) was maximal at 680 nm in the range 680 to 860 nm (Figure 6B). The absorption spectrum was in agreement with free SP2, indicating a good stability of SP2 within the composite. The PA intensity was not affected after mixing the composite with proteins while it increased upon bonding with BSA-SOH (bovine serum albumin with sulfenic acids), confirming efficient detection capacities of oxidative stress (Figure 6C). In xenografted HeLa tumor mouse model (Figure 6D), the PA signal of rSPN2 reach high intensity after 36 h of injection, which is 1.3-fold higher than control (SPN2) and 2.2-fold higher than the PA background signal of tumor.

Reactive oxygen species (ROS) production is another trait related to cancer. Cormode et al. have recently reported the design of hybrid nanogels for ROS imaging.[42] As shown in Figure 7A, such a system is based on a ROS sensitive nanogel, formed by poly[di(carboxylatophenoxy)phosphazene] (PCPP) and

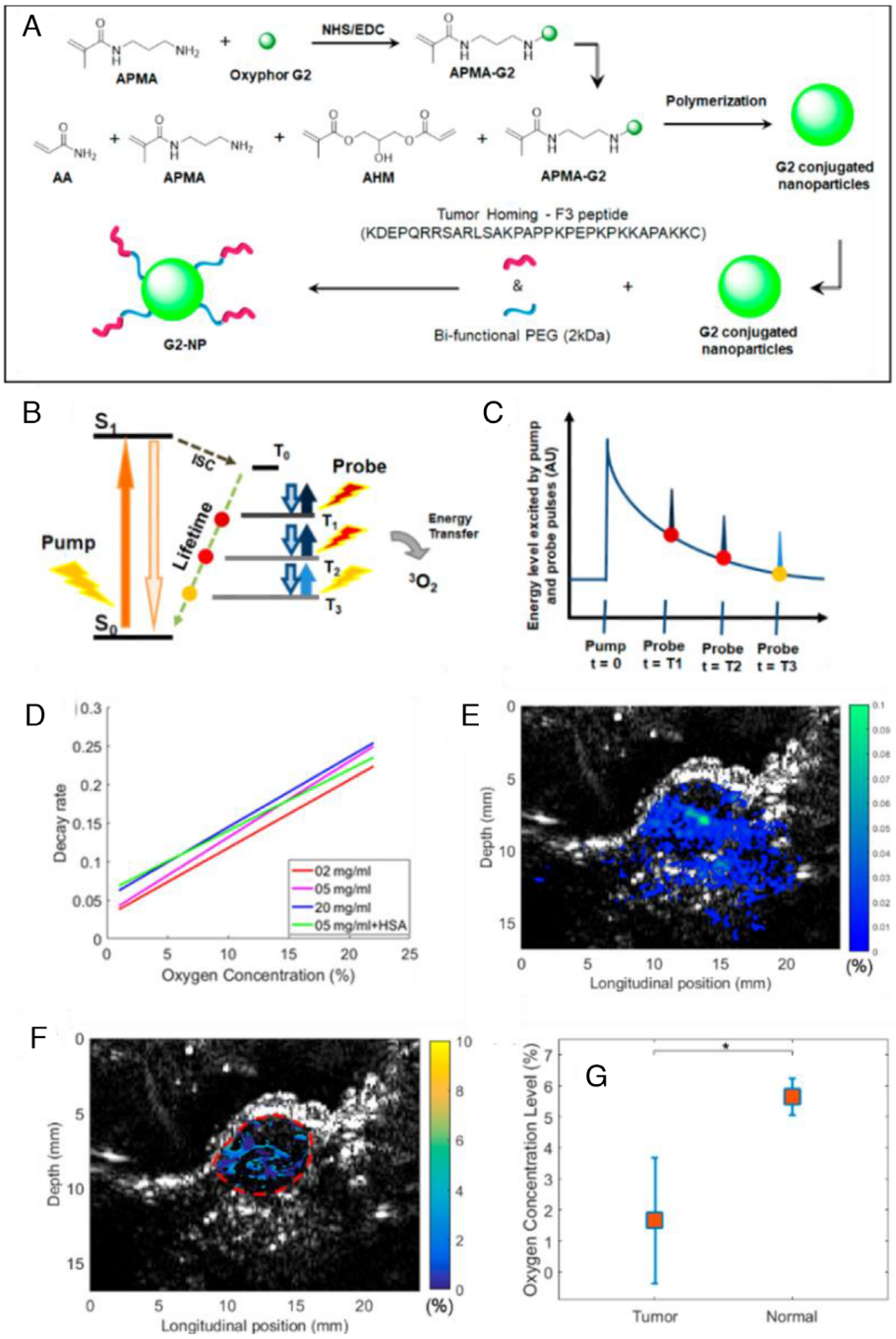

FIGURE 5 (A) Representative scheme of the synthesis of G2-PAA NPs, conjugated to F3 peptide. Illustration of PALT method: (B) the dye molecule is excited by a pump pulse from S_0 to S_1 and the energy transferred to the triplet state T_0. Subsequently, probe pulses detect the energy transfer from T_0 to ambient oxygen at different time points. (C) The phosphorescence decay curve can be established by varying the delay times between the pump and the probe pulses. (D) The decay rate is linearly correlated to oxygen concentration, as shown by the quantified decay rates as a function of the oxygen concentration. (E) PA imaging of G2-PAA NPs distribution and (f) PALT oxygen mapping in tumor area (dashed cycle). (F) Measured average oxygen concentration in tumor and normal (ie, thigh) tissue (* represents $P < 0.01$). Reprinted with permission from Ref. [35]. Copyright (2019) American Chemical Society

arylboronate polyphosphazene derivative (PPB), loading densely packed ultra-small Au NPs (<5 nm). The scaffold exhibits ROS-triggered degradation, releasing Au NPs and, thus, resulting in a significant decrease of the PA signal due to plasmon band shifting out of the NIR region. By comparing the PA to CT signal, ratiometric ROS imaging could be established for in vitro model of inflammation of LPS-stimulated macrophages (Figure 7B).

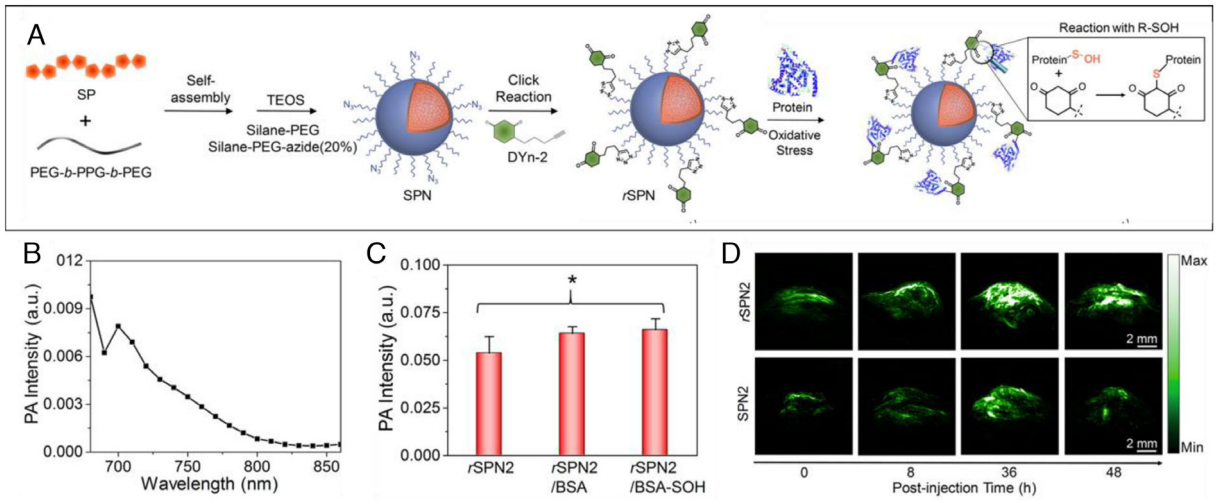

FIGURE 6 (A) Representative scheme of the synthesis of rSPN and mechanism of protein sulfonic acid detection. SP = SP2 = poly[2,6-(4,4-bis(2-ethylhexyl)-4H-cyclopenta[2,1-b;3,4-b]-dithiophene)-alt-4,7(2,1,3-benzothiadiazole)]; TEOS = tetraethyl orthosilicate, DYn-2 = 4-(pent-4-yn-1-yl)cyclohexane-1,3-dione, protein = BSA. (B) PA spectrum of rSPN2 (23 μg/mL of SP2 contrast agent) in buffer solution at pH = 7.4. (C) PA intensity at 680 nm of rSPN2, rSPN2 with BSA, and rSPN2 with BSA-SOH. (D) In vivo PA imaging of protein sulfonic acid in xenografted HeLa tumor mouse model after tail vein injection of rSPN2 and SPN2. Reprinted with permission from Ref. [60]. Copyright (2017) American Chemical Society

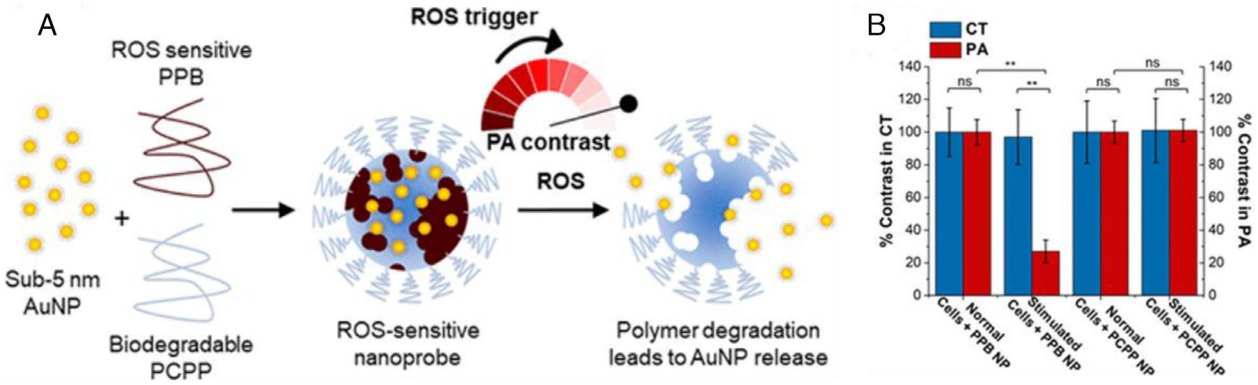

FIGURE 7 (A) Illustration of ROS-sensitive hybrid nanogels. The degradation of the nanogels takes place with ROS, releasing ultra-small Au NPs and decreasing PA signal. (B) Comparison between PA and CT signals of normal and stimulated RAW264.7 cells incubated with PPB (ROS-sensitive hybrid nanogel) and PCPP NPs (PCPP nanogels encapsulated Au NPs). Reprinted with permission from Ref. [42]. Copyright (2019) American Chemical Society

4 | CONCLUSION AND PERSPECTIVES

This article provides an up-to-date review on the development of nano- and microgels doped with PA contrast agents for PAI in cancer theranostics. Thanks to the loading of PA contrast agents, the hybrid microgels possess the capacity to convert NIR light to heat, a valuable feature for both PAI and phototherapy. In turn, the microgel network offers a protective matrix to improve the stability and biocompatibility of the trapped PA contrast agents. It also prevents their fast clearance by the reticuloendothelial system while fostering passive targeting of tumor by enhanced permeability and retention effect or active targeting via conjugation to ligands. Moreover, the stimuli-responsive properties of the hydrogel matrix offer unprecedented opportunities to achieve smart multifunctional platforms.

Nevertheless, this rapidly expanding research area is still in its infancy concerning clinical applications. There remain several challenges that need to be addressed before contrast agents based on hybrid microgels achieve their full potential for PAI. From a chemical point of view, there is still much room for improvement to fully control (i) the loading capacity of the microgel matrices, (ii) their size dispersity, and (iii) their biodegradability. It will be also crucial to get new insights into the stability of the trapped PA contrast agents within the smart microgel network to avoid their uncontrolled leakage before reaching the tumor target tissue. Another important challenge is related to the optical properties of the hybrid microgels, usually

settling across the first infrared window NIR-I (650 to 1000 nm). Designing nanocomposites with responsiveness in the NIR-II window (1000 to 1700 nm) will be the focus of future research, due to numerous advantages such as reduced optical absorption and tissue scattering together with deeper penetration depth. From a practical perspective, there is still a long way to go from basic research to clinical applications. This will rely on the design of hybrid microgel PA contrast agents with long-term stability in various environments and controlled pharmacodynamics, pharmacokinetics, and safety properties in vivo.

CONFLICT OF INTEREST

The authors declare that they have no conflict of interest.

ACKNOWLEDGMENT

We gratefully acknowledge the financial support from the ChinaScholarship Council (Yu Xiao's PhD fellowship). This work was partly funded by France Life Imaging (Grant No. ANR-11-INBS-0006), IdEx Université de Paris, ANR-18-IDEX-0001 (plateforme IVETh) and by the Region Ile de France under the convention SESAME 2019-IVETh (n° EX047011).

ORCID

Jérôme Gateau https://orcid.org/0000-0001-5230-8988
Amanda K A Silva https://orcid.org/0000-0002-7713-1813
Xiangyang Shi https://orcid.org/0000-0001-6785-6645
Florence Gazeau https://orcid.org/0000-0002-6482-3597
Claire Mangeney https://orcid.org/0000-0002-9817-3262
Yun Luo https://orcid.org/0000-0002-9515-0460

REFERENCES

1. A. G. Bell, *Science* **1881**, *2*, 242.
2. S. Wang, J. Lin, T. Wang, X. Chen, P. Huang, *Theranostics* **2016**, *6*, 2394.
3. K. Huang, Y. Zhang, J. Lin, P. Huang, *Biomater. Sci.* **2019**, *7*, 472.
4. S. Jiang, K. Huang, J. Qu, J. Lin, P. Huang, *View* **2021**, *2*, 20200075.
5. L. Lin, P. Hu, J. Shi, C. M. Appleton, K. Maslov, L. Li, R. Zhang, L. V. Wang, *Nat. Comm.* **2018**, *9*, 2352.
6. L. V. Wang, S. Hu, *Science* **2012**, *335*, 1458.
7. A. Ray, H. K. Yoon, Y. E. Koo Lee, R. Kopelman, X. Wang, *Analyst* **2013**, *138*, 3126.
8. P. Beard, *Interface Focus* **2011**, *1*, 602.
9. M. Schwarz, A. Buehler, J. Aguirre, V. Ntziachristos, *J. Biophotonics* **2016**, *9*, 55.
10. I. Stoffels, S. Morscher, I. Helfrich, U. Hillen, J. Leyh, N. C. Burton, T. C. Sardella, J. Claussen, T. D. Poeppel, H. S. Bachmann, A. Roesch, K. Griewank, D. Schadendorf, M. Gunzer, J. Klode, *Sci. Transl. Med.* **2015**, *7*, 317ra199.
11. X. Yang, E. W. Stein, S. Ashkenazi, L. V. Wang, *Wiley Interdiscip. Rev. Nanomed. Nanobiotechnol.* **2009**, *1*, 360.
12. Y. Zhou, Y. Hu, W. Sun, B. Zhou, J. Zhu, C. Peng, M. Shen, X. Shi, *Nanoscale* **2017**, *9*, 12746.
13. C. Zhang, X. Shi, in *Photonanotechnology for Therapeutics and Imaging* (Ed.: S. K. Choi), Elsevier **2020**, p. 23.
14. L. Jiang, Q. Zhou, K. Mu, H. Xie, Y. Zhu, W. Zhu, Y. Zhao, H. Xu, X. Yang, *Biomaterials* **2013**, *34*, 7418.
15. S. Peng, B. Ouyang, Y. Xin, W. Zhao, S. Shen, M. Zhan, L. Lu, *Acta Pharm. Sin. B* **2021**, *11*, 560.
16. L. Kong, F. Campbell, A. Kros, *Nanoscale Horiz.* **2019**, *4*, 378.
17. R.-M. Jin, M.-H. Yao, J. Yang, D.-H. Zhao, Y.-D. Zhao, B. Liu, *ACS Sustainable Chem. Eng.* **2017**, *5*, 9841.
18. D.-H. Zhao, J. Yang, R.-X. Xia, M.-H. Yao, R.-M. Jin, Y.-D. Zhao, B. Liu, *Chem. Comm.* **2018**, *54*, 527.
19. R. Jin, X. Yang, D. Zhao, X. Hou, C. Li, X. Song, W. Chen, Q. Wang, Y. Zhao, B. Liu, *Nanoscale* **2019**, *11*, 16080.
20. K. Miki, T. Inoue, Y. Kobayashi, K. Nakano, H. Matsuoka, F. Yamauchi, T. Yano, K. Ohe, *Biomacromolecules* **2015**, *16*, 219.
21. H. Wang, S. Mukherjee, J. Yi, P. Banerjee, Q. Chen, S. Zhou, *ACS Appl. Mater. Interfaces* **2017**, *9*, 18639.
22. Y. Zhai, W. Ran, J. Su, T. Lang, J. Meng, G. Wang, P. Zhang, Y. Li, *Adv. Mater.* **2018**, *30*, 1802378.
23. Y. Zhou, Y. Hu, W. Sun, S. Lu, C. Cai, C. Peng, J. Yu, R. Popovtzer, M. Shen, X. Shi, *Biomacromolecules* **2018**, *19*, 2034.
24. C. Zhang, W. Sun, Y. Wang, F. Xu, J. Qu, J. Xia, M. Shen, X. Shi, *ACS Appl. Mater. Interfaces* **2020**, *12*, 9107.
25. W. Li, X. Wang, J. Wang, Y. Guo, S. Y. Lu, C. M. Li, Y. Kang, Z. G. Wang, H. T. Ran, Y. Cao, H. Liu, *Biomacromolecules* **2019**, *20*, 401.
26. S. Biffi, L. Petrizza, C. Garrovo, E. Rampazzo, L. Andolfi, P. Giustetto, I. Nikolov, G. Kurdi, M. B. Danailov, G. Zauli, P. Secchiero, L. Prodi, *Int. J. Nanomed.* **2016**, *11*, 4865.
27. Z. Zhang, X. Zhang, Y. Ding, P. Long, J. Guo, C. Wang, *Macromol. Biosci.* **2019**, *19*, 1800416.
28. W. Huang, T. Leng, M. Gao, Q. Hu, L. Liu, H. Dou, *Carbohydr. Polym.* **2020**, *241*, 116224.
29. S. Zhang, W. Guo, J. Wei, C. Li, X. J. Liang, M. Yin, *ACS Nano* **2017**, *11*, 3797.
30. Y. Xu, J. Chen, L. Tong, P. Su, Y. Liu, B. Gu, B. Bao, L. Wang, *J. Controlled Release* **2019**, *293*, 94.
31. J. Jo, C. H. Lee, R. Kopelman, X. Wang, *Nat. Comm.* **2017**, *8*, 471.
32. L. E. Theune, J. Buchmann, S. Wedepohl, M. Molina, J. Laufer, M. Calderón, *J. Controlled Release* **2019**, *311*, 147.
33. P. A. Vasey, S. B. Kaye, R. Morrison, C. Twelves, P. Wilson, R. Duncan, A. H. Thomson, L. S. Murray, T. E. Hilditch, T. Murray, S. Burtles, D. Fraier, E. Frigerio, J. Cassidy, *Clin. Cancer Res.* **1999**, *5*, 83.
34. A. MaHam, Z. Tang, H. Wu, J. Wang, Y. Lin, *Small* **2009**, *5*, 1706.
35. J. Jo, C. H. Lee, J. Folz, J. W. Y. Tan, X. Wang, R. Kopelman, *ACS Nano* **2019**, *13*, 14024.
36. K. Sano, M. Ohashi, K. Kanazaki, N. Ding, J. Deguchi, Y. Kanada, M. Ono, H. Saji, *Biochem. Biophys. Res. Commun.* **2015**, *464*, 820.
37. Y. Tsunoi, S. Sato, S. Kawauchi, H. Ashida, D. Saitoh, M. Terakawa, *Burns* **2013**, *39*, 1403.
38. M. Jeon, W. Song, E. Huynh, J. Kim, J. Kim, B. L. Helfield, B. Y. Leung, D. E. Geortz, G. Zheng, J. Oh, *J. Biomed. Opt.* **2014**, *19*, 016005.
39. S. Park, J. Kim, M. Jeon, J. Song, C. Kim, *Sensors* **2014**, *14*, 19660.
40. J. Weber, P. C. Beard, S. E. Bohndiek, *Nat. Methods* **2016**, *13*, 639.
41. Y.-S. Chen, S. J. Yoon, W. Frey, M. Dockery, S. Emelianov, *Nat. Comm.* **2017**, *8*, 15782.

42. M. Bouche, M. Puhringer, A. Iturmendi, A. Amirshaghaghi, A. Tsourkas, I. Teasdale, D. P. Cormode, *ACS Appl. Mater. Interfaces* **2019**, *11*, 28648.
43. J. Ge, Q. Jia, W. Liu, L. Guo, Q. Liu, M. Lan, H. Zhang, X. Meng, P. Wang, *Adv. Mater.* **2015**, *27*, 4169.
44. A. d. l. Zerda, Z. Liu, S. Bodapati, R. Teed, S. Vaithilingam, B. T. Khuri-Yakub, X. Chen, H. Dai, S. S. Gambhir, *Nano Lett.* **2010**, *10*, 2168.
45. Z. Sheng, L. Song, J. Zheng, D. Hu, M. He, M. Zheng, G. Gao, P. Gong, P. Zhang, Y. Ma, L. Cai, *Biomaterials* **2013**, *34*, 5236.
46. L. Feng, C. Zhu, H. Yuan, L. Liu, F. Lv, S. Wang, *Chem. Soc. Rev.* **2013**, *42*, 6620.
47. K. Pu, N. Chattopadhyay, J. Rao, *J. Controlled Release* **2016**, *240*, 312.
48. G. Eskiizmir, A. T. Ermertcan, K. Yapici, in *Nanostructures for Oral Medicine* (Eds.: E. Andronescu, A. M. Grumezescu), Elsevier **2017**, p. 511.
49. Y. Liu, P. Bhattarai, Z. Dai, X. Chen, *Chem. Soc. Rev.* **2019**, *48*, 2053.
50. Y. Lyu, J. Li, K. Pu, *Small Methods* **2019**, *3*, 1900553.
51. G. Wang, F. Zhang, R. Tian, L. Zhang, G. Fu, L. Yang, L. Zhu, *ACS Appl. Mater. Interfaces* **2016**, *8*, 5608.
52. X. Liang, Y. Li, X. Li, L. Jing, Z. Deng, X. Yue, C. Li, Z. Dai, *Adv. Funct. Mater.* **2015**, *25*, 1451.
53. Q. Tian, Y. Li, S. Jiang, L. An, J. Lin, H. Wu, P. Huang, S. Yang, *Small* **2019**, *15*, 1902926.
54. G. Lalwani, X. Cai, L. Nie, L. V. Wang, B. Sitharaman, *Photoacoustics* **2013**, *1*, 62.
55. G. Chen, B. Ma, Y. Wang, R. Xie, C. Li, K. Dou, S. Gong, *ACS Appl. Mater. Interfaces* **2017**, *9*, 41700.
56. S. Lu, X. Li, J. Zhang, C. Peng, M. Shen, X. Shi, *Adv. Sci.* **2018**, *5*, 1801612.
57. C. Cai, X. Li, Y. Wang, M. Liu, X. Shi, J. Xia, M. Shen, *Chem. Eng. J.* **2019**, *362*, 842.
58. T. Yang, Y. Tang, L. Liu, X. Lv, Q. Wang, H. Ke, Y. Deng, H. Yang, X. Yang, G. Liu, Y. Zhao, H. Chen, *ACS Nano* **2017**, *11*, 1848.
59. Z. Ouyang, D. Li, Z. Xiong, C. Song, Y. Gao, R. Liu, M. Shen, X. Shi, *ACS Appl. Mater. Interfaces* **2021**, *13*, 6069.
60. Y. Lyu, X. Zhen, Y. Miao, K. Pu, *ACS Nano* **2017**, *11*, 358.
61. D. Hanahan, R. A. Weinberg, *Cell* **2000**, *100*, 57.
62. D. Hanahan, R. A. Weinberg, *Cell* **2011**, *144*, 646.
63. M. Jafari, M. Hasanzadeh, *Biomed. Pharmacother.* **2020**, *122*, 109770.
64. F. A. Gallagher, M. I. Kettunen, S. E. Day, D.-E. Hu, J. H. Ardenkjær-Larsen, P. R. Jensen, M. Karlsson, K. Golman, M. H. Lerche, K. M. Brindle, *Nature* **2008**, *453*, 940.
65. M. W. Dewhirst, S. R. Birer, *Cancer Res.* **2016**, *76*, 769.
66. R. S. Frackowiak, G. L. Lenzi, T. Jones, J. D. Heather, *J. Comput. Assist. Tomogr.* **1980**, *4*, 727.
67. A. L. Vāvere, G. B. Biddlecombe, W. M. Spees, J. R. Garbow, D. Wijesinghe, O. A. Andreev, D. M. Engelman, Y. K. Reshetnyak, J. S. Lewis, *Cancer Res.* **2009**, *69*, 4510.
68. X. D. Wang, O. S. Wolfbeis, *Chem. Soc. Rev.* **2014**, *43*, 3666.
69. Y. H. Seo, K. S. Carroll, *Proc. Natl. Acad. Sci. U.S.A.* **2009**, *106*, 16163.
70. Mikhail Y. Berezin, K. Guo, W. Akers, Ralph E. Northdurft, Joseph P. Culver, B. Teng, O. Vasalatiy, K. Barbacow, A. Gandjbakhche, Gary L. Griffiths, S. Achilefu, *Biophys. J.* **2011**, *100*, 2063.
71. M. Hockel, P. Vaupel, *J. Natl. Cancer Inst.* **2001**, *93*, 266.
72. Y. Kato, S. Ozawa, C. Miyamoto, Y. Maehata, A. Suzuki, T. Maeda, Y. Baba, *Cancer Cell Int.* **2013**, *13*, 89.
73. N. Raghunand, X. He, R. v. Sluis, B. Mahoney, B. Baggett, C. W. Taylor, G. Paine-Murrieta, D. Roe, Z. M. Bhujwalla, R. J. Gillies, *Br. J. Cancer* **1999**, *80*, 1005.
74. O. Trédan, C. M. Galmarini, K. Patel, I. F. Tannock, *J. Natl. Cancer. Inst.* **2007**, *99*, 1441.
75. Q. Chen, X. Liu, J. Chen, J. Zeng, Z. Cheng, Z. Liu, *Adv. Mater.* **2015**, *27*, 6820.
76. S. Guha, G. K. Shaw, T. M. Mitcham, R. R. Bouchard, B. D. Smith, *Chem. Comm.* **2016**, *52*, 120.
77. C. W. Kimbrough, A. Khanal, M. Zeiderman, B. R. Khanal, N. C. Burton, K. M. McMasters, S. M. Vickers, W. E. Grizzle, L. R. McNally, *Clin. Cancer Res.* **2015**, *21*, 4576.
78. J. Han, K. Burgess, *Chem. Rev.* **2010**, *110*, 2709.
79. V. Petrova, M. Annicchiarico-Petruzzelli, G. Melino, I. Amelio, *Oncogenesis* **2018**, *7*, 10.
80. H. Zhong, A. M. De Marzo, E. Laughner, M. Lim, D. A. Hilton, D. Zagzag, P. Buechler, W. B. Isaacs, G. L. Semenza, J. W. Simons, *Cancer Res.* **1999**, *59*, 5830.
81. P. H. Maxwell, M. S. Wiesener, G.-W. Chang, S. C. Clifford, E. C. Vaux, M. E. Cockman, C. C. Wykoff, C. W. Pugh, E. R. Maher, P. J. Ratcliffe, *Nature* **1999**, *399*, 271.
82. S. Tzoumas, A. Nunes, I. Olefir, S. Stangl, P. Symvoulidis, S. Glasl, C. Bayer, G. Multhoff, V. Ntziachristos, *Nat. Comm.* **2016**, *7*, 12121.
83. T. Fiaschi, P. Chiarugi, *Int. J. Cell Biol.* **2012**, *2012*, 762825.
84. L. Raj, T. Ide, A. U. Gurkar, M. Foley, M. Schenone, X. Li, N. J. Tolliday, T. R. Golub, S. A. Carr, A. F. Shamji, A. M. Stern, A. Mandinova, S. L. Schreiber, S. W. Lee, *Nature* **2011**, *475*, 231.
85. O. Rudyk, P. Eaton, *Redox Biol.* **2014**, *2*, 803.

AUTHOR BIOGRAPHIES

Yu Xiao received her Master's degree from West China Medical Center in 2018. She is a PhD candidate in LCBPT lab (CNRS UMR 8601), Université de Paris under supervision of Prof. Claire Mangeney and Dr. Florence Gazeau, working on multimodal drug delivery system for cancer therapy, novel functional nanomaterials for SERS, photothermal therapy, and photoacoustic imaging.

Florence Gazeau completed her PhD degree in physics in 1997 focusing on the magnetic and hydrodynamic properties of ferrofluids. She is a Senior Scientist in CNRS, group leader MSC Med and Deputy Director of the laboratory Matière et Systèmes Complexes (MSC) at the Université de Paris. Her main research interest includes nanomagnetism and nanomedicine: interac-

tions of nanoparticles with the biological environment, Imaging contrast agent nanoparticles-mediated hyperthermia, biotransformation and fate of nanomaterials in the organism and cell therapy and extracellular vesicles as drug delivery systems. She is author of 160 publications, inventors of eight patents, and cofounder of the company EVORA Biosciences.

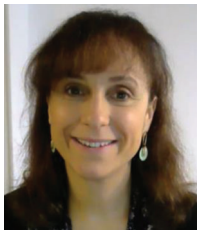

Claire Mangeney is full professor at Université de Paris, LCBPT lab (CNRS UMR 8601), Université de Paris. Her research interest is at the interface of surface chemistry, nanotechnology, and biology. Her primary goal is to develop innovative hybrid nanomaterials for nanomedecine and to integrate them into theranostic agents or advanced "all optical" sensing devices for biological-related applications.

Yun Luo obtained her PhD from INSA de Rennes (France) in 2012. She is a CNRS researcher (CRCN) since 2019 in LCBPT lab (CNRS UMR 8601), Université de Paris. Her research interests focus on advance nanomaterials for energy conversion, surface functionalization of nanomaterials for biomedical applications, for example, multimodal bioimaging, multifunctional drug delivery system, nanomedicine and implant devices.

How to cite this article: Xiao Y, Gateau J, Silva AKA, Shi X, Gazeau F, Mangeney C, Luo Y. *VIEW* **2021**; 20200176.
https://doi.org/10.1002/VIW.20200176